Atmos. Meas. Tech. Discuss., doi:10.5194/amt-2016-63, 2016
Manuscript under review for journal Atmos. Meas. Tech.
Published: 15 March 2016

Atmospheric Measurement Techniques Discussions

Global distributions of CO_2 volume mixing ratio in the middle and upper atmosphere from MIPAS high resolution spectra

Á. Aythami Jurado-Navarro[1], Manuel López-Puertas[1], Bernd Funke[1], Maya García-Comas[1], Angela Gardini[1], Francisco González-Galindo[1], Gabriele P. Stiller[2], Thomas v. Clarmann[2], Udo Grabowski[2], and Andrea Linden[2]

[1]Instituto de Astrofísica de Andalucía, CSIC, Granada, Spain
[2]Institute for Meteorology and Climate Research (IMK-ASF), Karlsruhe Institute of Technology (KIT), Karlsruhe, Germany
Correspondence to: M. López-Puertas (puertas@iaa.es)

Abstract. Global distributions of the CO_2 vmr (volume mixing ratio) in the mesosphere and lower thermosphere (from 70 km up to ∼142 km) have been derived from high resolution mid-IR spectra. This is the first time that the CO_2 vmr has been retrieved in the 120–140 km range. The CO_2 vmrs have been retrieved using MIPAS daytime limb emission spectra from the 4.3 μm region in its upper atmosphere (UA) mode (data version v5r_CO2_622). The dataset spans from January 2005 until March 2012. The retrieval of CO_2 has been performed jointly with the line of sight (LOS) by using a non-local thermodynamic equilibrium (non-LTE) retrieval scheme. The non-LTE model incorporates the accurate vibrational-vibrational and vibrational-translational collisional rates recently derived from the MIPAS spectra. It also takes advantage of simultaneous MIPAS measurements of other atmospheric parameters, as the kinetic temperature (up to ∼100 km) from the CO_2 15 μm region, the thermospheric temperature from the NO 5.3 μm emission, and the O_3 measurements (up to ∼100 km). The latter is very important for the calculations of the non-LTE populations because it strongly constrains the O(^1D) concentration below ∼100 km. The estimated precision of the retrieved CO_2 vmr profiles varies with altitude ranging from ∼1% below 90 km, to 5% around 120 km and larger than 10% above 130 km. There are some latitudinal and seasonal variations of the precision, which are mainly driven by the solar illumination conditions. The retrieved CO_2 profiles have a vertical resolution of about 5–7 km below 120 km and between 10 and 20 km at 120–142 km. We have shown that the inclusion of the LOS as joint fit parameter improves the retrieval of CO_2, allowing a clear discrimination between the information of CO_2 concentration and the LOS and also leading to significantly smaller systematic errors. The retrieved CO_2 has a much better accuracy than previous limb emission measurements, because of the highly accurate rate coefficients recently derived from MIPAS, and the simultaneous MIPAS measurements of other key atmospheric parameters needed for the non-LTE modeling like the kinetic temperature and the O_3 concentration. The major systematic error source is the uncertainty of the pressure/temperature profiles, inducing errors of up to 15% above 100 km, and of ∼5% around 80 km at mid-latitude conditions. The errors due to uncertainties in the O(^1D) and O(^3P) profiles are within 3–4% in the 100–120 km region, and those due to uncertainties in the gain calibration and in the near-IR solar flux are within ∼2% at all altitudes. The retrieved CO_2 shows the major features expected and predicted by general circulation models. In particular, its abrupt decline above 80–90 km and the seasonal change of the latitudinal distribution, with higher CO_2 abundances in polar summer from 70 km up to ∼95 km and lower CO_2 vmr in the polar winter. Above

Atmos. Meas. Tech. Discuss., doi:10.5194/amt-2016-63, 2016
Manuscript under review for journal Atmos. Meas. Tech.
Published: 15 March 2016

Atmospheric Measurement Techniques Discussions

~95 km, CO_2 is more abundant in the polar winter than at mid-latitudes and polar summer regions, caused by the reversal of the mean circulation in that altitude region. Also, the solstice seasonal distribution, with a significant pole-to-pole CO_2 gradient, lasts about 2.5 months in each hemisphere, while the seasonal transition occurs quickly.

1 Introduction

Carbon dioxide, CO_2, plays a major role in the radiative energy budget of the atmosphere. Its 15 μm is the major infrared cooling below around 120 km, and it also causes a significant heating of the upper mesosphere by the absorption of solar radiation in its near-IR bands (see, e.g. López-Puertas and Taylor, 2001). Hence, CO_2 has a critical effect on the atmospheric temperature structure and therefore it is very important to know accurately its global (altitude and latitude) distribution (see, e.g. Garcia et al., 2014).

CO_2 was first measured in the upper atmosphere by *in situ* measurements carried out by rocket-borne mass spectrometers (Offermann and Grossmann, 1973; Trinks et al., 1978; Trinks and Fricke, 1978). The Spectral Infrared Rocket Experiment (SPIRE) measured its 15 μm non-LTE (non-Local Thermodynamic Equilibrium) emission (Stair et al., 1985). The improved Stratospheric and Mesospheric Sounder (ISAMS) aboard Upper Atmosphere Research Satellite (UARS) carried out 4.6 μm global measurements performing simultaneous measurements of temperature and pressure up to 80 km (López-Puertas et al., 1998; Zaragoza et al., 2000). CO_2 number densities were retrieved from daytime limb radiance measured by the Cryogenic Infrared Spectrometers and Telescopes for the Atmosphere (CRISTA) measurements in the 60–130 km region (Kaufmann et al., 2002). For a complete review of early measurements until 2000 see López-Puertas et al. (2000). More recently, two satellite CO_2 datasets have been made available. The Fourier Transform Spectrometer on the Canadian Atmospheric Chemistry Experiment (ACE-FTS) has measured the CO_2 vmr in mesosphere and lower thermosphere (70 to 120 km) by using the solar occultation technique. This approach has the advantage of being free from non-LTE effects (and the errors associated to the knowledge of the non-LTE population of the emitting states) but, on the other hand, provides a limited latitudinal coverage (Beagley et al., 2010). Almost simultaneously with ACE, the Sounding of the Atmosphere using Broadband Emission Radiometry (SABER), on board the NASA Thermosphere Ionosphere Energetics and Dynamics (TIMED), has been measuring the atmospheric limb radiance in the 15 μm and 4.3 μm channels. Rezac et al. (2015) have applied a simultaneous temperature–CO_2 vmr retrieval to these measurements and produced an long (13 years) database of CO_2 in the middle and upper atmosphere.

In this paper we describe the inversion of CO_2 vmr from MIPAS high resolution limb emission spectra in the 4.3 μm region. MIPAS is able to discriminate the contributions of the many CO_2 bands that gives rise to the 4.3 μm atmospheric emission; and thus has allowed us to obtain a very accurate knowledge of the CO_2 non-LTE processes that control the population of the emitting levels near 4.3 μm (Jurado-Navarro et al., 2015). This has a direct impact on the retrieved CO_2 presented here which has a much better accuracy than previous limb emission measurements.

In Section 2 we describe the MIPAS instrument, and the measurements and in Sec. 3 the retrieval method. The advantages of using the CO_2-LOS (line of sight) joint retrieval are discussed in Sec. 4. In Sec. 5 we discuss the major characteristics of the retrieved CO_2 vmr and the error analysis. Finally, in Sec. 6 we provide and discuss a monthly climatology based on the data

Atmos. Meas. Tech. Discuss., doi:10.5194/amt-2016-63, 2016
Manuscript under review for journal Atmos. Meas. Tech.
Published: 15 March 2016

Atmospheric Measurement Techniques Discussions

retrieved in 2010 and 2011. A validation and comparison of MIPAS CO_2 data with ACE and SABER measurements, as well as with Whole Atmosphere Community Climate Model (WACCM) simulations is foreseen to be presented in a future paper.

2 MIPAS observations

The MIPAS instrument is a mid-infrared limb emission spectrometer designed and operated for measurement of atmospheric trace species from space (Fischer et al., 2008). It was part of the payload of Envisat launched on 1 March 2002 with a sun-synchronous polar orbit of 98.55°N inclination and an altitude of 800 km. MIPAS had a global coverage from pole to pole passing the equator from north to south at 10:00 a.m. local time 14.3 times a day and taking daytime and nighttime profiles of spectra. The instrument's field-of-view is 30 km in horizontal and approximately 3 km in vertical direction. From January 2005 until the end of Envisat's operations on 8 April 2012, MIPAS measured at a optimized spectral resolution of 0.0625 cm^{-1}.

The MIPAS instrument sounded the middle and upper atmospheres in three measurements modes: MA, UA and NLC. The UA mode, scanning the limb from 42 to 172 km, was specifically devised for measuring the thermospheric temperature and CO_2 and NO abundances. In the MA and NLC modes, MIPAS took spectra up to 102 km only. However, since many lines of the CO_2 bands are still optically thick at this tangent height and above, they reduce the sensitivity to the retrieved CO_2 below 102 km. Thus, having measurements above that altitude are very important to retrieve the CO_2 in the optically thin regime and hence better constrain the CO_2 vmr below. In consequence, the retrieval setup and the derived CO_2 presented here, data version v5r_CO2_622, correspond to the UA observation mode. Only daytime data were used since the nighttime observations are very noisy and non-LTE is not known so accurately. Note that the three MIPAS modes have very similar temporal and latitudinal coverages. Hence the retrieval of CO_2 from the MA and NLC modes would not extent significantly the coverage of the CO_2 UA database. The limb vertical sampling of the UA mode is 5 km from 172 km down to 102 km, and 3 km below, recording a rear viewing sequence of 35 spectra every 63 s. Its along-tracking horizontal sampling of about 515 km (De Laurentis, 2005; Oelhaf, 2008). Version V5 (5.02/5.06) of the L1b calibrated and geo-located spectra processed by the European Space Agency (ESA) were used here (Perron et al., 2010; Raspollini et al., 2010).

3 The retrieval method

Carbon dioxide vmr profiles together with the line of sight (LOS) altitude information are retrieved using the MIPAS level 2 processor developed and operated by the Institute of Meteorology and Climate Research (IMK) together with the Instituto de Astrofísica de Andalucía (IAA). The processor is based on a constrained non-linear least squares algorithm with Levenberg-Marquardt damping (von Clarmann et al., 2003). Its extension to retrievals with consideration of non-LTE (i.e. CO, NO, and NO_2) is described in Funke et al. (2001). Non-LTE vibrational populations of CO_2 are modeled with the Generic RAdiative traNsfer AnD non-LTE population Algorithm (GRANADA) (Funke et al., 2012) (see more details below) within each iteration of the retrieval. Calculated spectra are fitted to the measured ones in an iterative way by updating the actual vector of the retrieved quantities. In order to stabilize the retrieval, a priori assumptions are used. The *a priori* profile of CO_2 is taken from

Atmos. Meas. Tech. Discuss., doi:10.5194/amt-2016-63, 2016
Manuscript under review for journal Atmos. Meas. Tech.
Published: 15 March 2016

Atmospheric Measurement Techniques Discussions

the Whole Atmosphere Community Climate Model with specified dynamics (SD-WACCM) simulations (Garcia et al., 2014). SD-WACCM is constrained with output from NASA's Modern-Era Retrospective Analysis (MERRA) (Rienecker et al., 2011) below approximately 1 hPa. Garcia et al. (2014) showed SD-WACCM simulations for Prandtl numbers (P_r) of 4 (standard) and 2, corresponding to lower and higher eddy diffusion coefficients, respectively. Here we used the simulations for P_r=2, which gives an overall better agreement with ACE CO and CO_2 and MIPAS CO (Garcia et al., 2014). The CO_2 profile is regularized by means of a Tikhonov-type (Tikhonov, 1963) smoothing constraint. A strong diagonal constrain is added below 60 km in order to force the retrieved CO_2 to be close to the well-known mixing ratio in the lower mesosphere. Above 60 km, the constrain is optimized to obtain stable calculations with a precision high enough to allow for meaningful physical interpretation of the retrieved CO_2 abundance.

The retrievals are performed using selected spectral regions (micro-windows) in the 4.3 μm region in MIPAS channel D (1820–2410 cm^{-1}), which vary with tangent altitude, in order to optimize computation time and minimize systematic errors (von Clarmann and Echle, 1998). In particular, error propagation due to horizontal inhomogeneities have been minimized by excluding opaque spectral lines which are insensitive to tangent point conditions.

The selection of the spectral regions sensitive to the CO_2 abundance is performed by calculating the 4.3 μm Jacobians and selecting those regions with a good local response. In this way, and thanks to the excellent MIPAS spectral resolution, we are able to select the spectral points sensitive to the CO_2 vmr, yet with a good signal-to-noise ratio, while excluding lines with non-local responses due to spectral saturation. We have selected 18 principal spectral regions within the 2300–2380 cm^{-1} range, containing height-dependent microwindows at 23 tangent heights from 60 km up to 142 km. An illustration of the selection for a particular spectral region is shown in Fig. 1. At 60 km, the fundamental band line (black) shows a local response and hence it is selected in the micro-windows mask. On the contrary, the second hot lines (red and orange) do not give a local response (the Jacobians are much extended in altitude or their maxima occur at altitudes well above the tangent height) and hence are not selected. They are, however, included in the microwindow mask for higher tangent heights, i.e. from 85 km up to 102 km, where they have quite enough local sensitivity. In this example the fundamental band line is not selected from 72 to 90 km, although it gives again valuable information at 102 km. Precisely, the 102 km altitude marks the transition height where the information from second hot band ends and that of the fundamental band starts.

In addition to the exclusion of spectral points with non-local response, we restricted the microwindows to the strongest lines (mainly fundamental and second hot bands lines that have the larger signal/noise ratio) at each altitude for reasons of computational efficiency. Additionally, spectral regions with interferences from the 636, 628, 627, 638 and 637 CO_2 isotopologues have been suppressed in order to avoid systematic errors caused by the less accurate non-LTE modeling of these minor species.

The resulting selection of microwindows (occupation matrix) is shown in Fig.2. The selected spectral points belong mainly to the lines of the fundamental band in the 60–72 km and 102–142 km regions, and of the second hot bands in the 75–102 km region. More detailed information on the microwindows used in the retrieval is given in the Supplement.

The *a priori* for the line of sight (LOS) was taken from that retrieved from the 15 μm region (García-Comas et al., 2014). A Tikhonov smoothing constraint is used for the LOS retrieval, allowing for vertically coarse variations of ∼10–20 km of the

Atmos. Meas. Tech. Discuss., doi:10.5194/amt-2016-63, 2016
Manuscript under review for journal Atmos. Meas. Tech.
Published: 15 March 2016

Atmospheric Measurement Techniques Discussions

tangent height spacing with respect to the *a priori*. The LOS of the lowermost tangent height is strongly constrained to the a priori by means of a diagonal regularization. Typically, the obtained degrees of freedom for the LOS retrievals are about 2.

Besides the CO_2 vmr profile and LOS, a height- and wavenumber-independent radiance offset is also fitted jointly in the retrieval. Before starting the retrieval, the L1b spectra were corrected for the spectral shift. The temperature used in the retrieval was taken from that retrieved from the same MIPAS spectra in the 15 μm region (García-Comas et al., 2014) below around 100 km, and that retrieved from the NO 5.3 μm emission Bermejo-Pantaleón et al. (2011) from 100 km up to 170 km.

Pressure was implicitly determined by means of hydrostatic equilibrium (total density was obtained from pressure and temperature and using the ideal gas law). The CO_2 non-LTE model used in the non-LTE inversion is described in detail in Funke et al. (2012). However, the collisional coefficients of many vibrational-vibrational and vibrational-translational processes were significantly updated with the values retrieved from MIPAS spectra as described in Jurado-Navarro et al. (2015). In addition, some of the collisional rates of that work were updated here because of the improvements in the calculation the O(^1D) concentration (see below) and further refinements leading to smaller residual spectra. The updates include, first, the collisional rates of $CO_2(v_d, v_3)$ + M $\leftrightharpoons$ $CO_2(v'_d, v_3 - 1)$ + M with Δv_d=2–4 and M=N_2, O_2 (processes 8a and 8b in Table 1 of Jurado-Navarro et al., 2015) where the factor f has been changed from 0.82 to 0.7. Secondly, the rate of $N_2(1)$ + O $\rightarrow$ N_2 + O (process 10 in that table) has been updated with a rate coefficient of 4.5×10^{-15} (T/300)$^{1.5}$ cm^{3}s^{-1} and f = 1. This rate has been adapted from Whitson and McNeal (1977) taking the upper limit (within the error bars) at 300 K and re-adjusting the temperature dependence taking into account the measurements at higher temperatures. The values of this new rate at temperatures near 300 K are, however, similar to those used in Jurado-Navarro et al. (2015).

The non-LTE model also requires other input quantities that affect the non-LTE populations of the emitting states. In particular it requires the concentrations of O_3, O(^3P) and O(^1D). For ozone we used that retrieved from the MIPAS spectra in the 10 μm spectral region (Gil-López et al., 2005) below around 100 km.

The atomic oxygen and O(^1D) profiles below 100 km were generated from the O_3 retrieved from MIPAS and the photochemical model described in (Funke et al., 2012). Above 100 km, we took the atomic oxygen and O_2 concentrations from the NRLMSIS-00 model (Picone et al., 2002). The O(^1D) profile above 100 km has been updated from the photochemical model of Funke et al. (2012) by using the O_2 photo-absorption cross sections of Ogawa and Ogawa (1975) and Lu et al. (2010), and a new efficiency of O(^1D) production from O_2 photo-absorption that consider that at wavelengths shorter than $\sim$100 nm the O_2 ionization is the dominant channel. Also, we included an overhead column above the top layer of the model proportional to the scale height of O_2. This O(^1D) photo-production has been compared with that calculated for similar conditions by an independent 1D model UV radiative transfer model (González-Galindo et al., 2005; Garcia et al., 2014) finding differences smaller than 2% at all altitudes. A variable solar spectral irradiance (SSI) (Lean et al., 2005) was included in all the photochemical calculations in order to account for solar UV variations along the MIPAS observation period.

Atmos. Meas. Tech. Discuss., doi:10.5194/amt-2016-63, 2016
Manuscript under review for journal Atmos. Meas. Tech.
Published: 15 March 2016

Atmospheric Measurement Techniques Discussions

4 Proof of concept of the CO_2-LOS joint retrieval

In order to test the performance of the retrieval setup we have applied it to synthetic spectra calculated with the Karlsruhe Optimized and Precise Radiative Transfer Algorithm (KOPRA) (Stiller et al., 2002) and non-LTE populations for the mid-latitude April 45°N daytime (SZA=44.5°) and for the polar summer January 75°S (SZA=58.7°) reference atmospheres (Funke et al., 2012; Jurado-Navarro et al., 2015). Typical MIPAS spectral noise was artificially added to the simulated measurements. We investigate the sensitivity of the retrieval of CO_2 vmr to the CO_2 and LOS *a priori* profiles separately. In particular we want to know if the retrieval yields reasonable results even when the CO_2 and LOS *a priori* are very different from the actual atmospheric and observational conditions.

The CO_2 *a priori* profile was perturbed by exchanging the corresponding SD-WACCM profiles of the two atmospheric conditions, i.e. the mid-latitude SD-WACCM profile was implemented in the polar summer input and vice versa. Under mid-latitude conditions, the retrieved CO_2 profile differs from the true value by less than 2–3% in the whole altitude region (Fig. 3a). Compared to the difference with the *a priori* profile (up to 35%), the agreement of the retrieved profile and the "true" is excellent. Regarding polar summer conditions, the differences between the retrieved and the true profiles are generally smaller than 2% except at 95 to 110 km where it ranges at 2–4% (Fig. 3b). We have also tested the effect of the *a priori* when retrieving only the CO_2 vmr and keeping fixed the LOS, i.e., with CO_2 as a single-parameter retrieval. The result is shown by the green line in Figs. 3a and 3b. We see that, for both atmospheric conditions, the differences between the retrieved CO_2 with and without the joint fit of LOS are only marginal. Also, the inspection of the retrieved LOS in the joint fit case (Fig. 4) shows that the mapping of the CO_2 *a priori* uncertainties on the LOS is very small (less than 20 m).

We also tested the impact of a perturbation of the LOS *a priori* information on the retrieved CO_2. We applied a sine function perturbation to the LOS with a value of 0 m at 60 km and 142 km and a maximum of 200 m at 90 km. Above 90 km, the use of the perturbed *a priori* LOS profile in the CO_2–LOS joint retrieval introduces deviations of the retrieved CO_2 from the true profile smaller than 1–2%, while differences are negligible below (see red line in Figs. 5a and 5b). On the other hand, the application of the perturbed LOS in the single-parameter CO_2 retrieval introduces a significant systematic error of up to 3–4% for mid-latitudes and even larger (up to 5%) for polar summer above 70 km (see green line in Figs. 5a and 5b).

In Section 5.2 we also discuss the effects of using the joint CO_2-LOS or the CO_2-only retrievals on the total systematic error, resulting in a notably larger uncertainty for the CO_2-only retrieval.

Therefore, these results give us confidence in the retrieval scheme and we conclude that the impact of *a priori* profile uncertainties on the retrieved CO_2 is very small, $\lesssim$1–2%. Furthermore, fitting the LOS jointly was found not to degrade the retrieved CO_2 mixing ratios while it avoids important systematic errors due to LOS uncertainties.

Figures 6a and 6b show the columns of the averaging kernel of the CO_2 vmr from the joint CO_2-LOS retrieval at several altitudes for the cases studied above for mid-latitudes and polar summer conditions. There are two clear regions with higher sensitivity, one ranging from around 75 to 95 km, and another from $\sim$105 to 135 km. In the lower region most of the information comes from the second hot bands (as discussed above), and in the upper region from the first and mainly from the fundamental 4.3 μm bands. There is a clear region in between where the sensitivity is smaller. It is also noticeable that even after the careful

Atmos. Meas. Tech. Discuss., doi:10.5194/amt-2016-63, 2016
Manuscript under review for journal Atmos. Meas. Tech.
Published: 15 March 2016

Atmospheric Measurement Techniques Discussions

selection of the microwindows is difficult to obtain information about the CO_2 vmr in the lowermost latitudes, below around 70–75 km. The averaging kernel row corresponding to the lowermost altitude shown in Figs. 6a and 6b, 72 km, maximizes a few kilometers above this altitude. It also has a long negative tail above 120 km, caused by the strong regularization applied to the CO_2 profile at its lower edge in conjunction with optically thick radiative transfer. The retrieval algorithm responds to a positive perturbation of the CO_2 in the strongly regularized profile range (below 70 km) with a reduction of the thermospheric CO_2 column (i.e., reduction of absorption). Similar features are shown for the averaging kernel rows corresponding to altitudes below 72 km. It is also evident the decrease of the vertical resolution above ∼120 km, with the averaging kernels becoming wider, partially due to the coarser measurement sampling.

5 Characterization of the retrieved CO_2 vmr

5.1 Precision and vertical resolution

The vertical resolution and the precision are two important diagnostic parameters for characterizing the quality of any retrieval. Fig. 7 shows the zonal means of these parameters calculated for each season using 3 months: December-January-February, March-April-May, June-July-August and September-October-November from the retrieved data from MIPAS measurements in the UA mode for 2010 and 2011. The zonal mean CO_2 distribution is also shown (left panels) for reference.

In general, the precision varies with altitude ranging from ∼1% below 90 km, 5% around 120 km and larger than 10% above 130 km. The larger values at higher altitudes are due to the lower signal-to-noise ratio. There are some latitudinal and seasonal variations, which are driven by the solar illumination conditions.

The vertical resolution is typically around 5–7 km below 120 km. Above that altitude, it is coarser, with values larger than 10 km, mainly caused by the coarser vertical sampling (5 km instead of 3 km).

Around ∼105 km, a slight degradation of the vertical resolution is observed. This altitude corresponds to the tangent height region where the microwindows include lines from the second hot bands only while the fundamental band lines are used above. The latter, as discussed above in Sec. 3, are still rather optically thick at these tangent heights and hence have been rejected.

5.2 Systematic errors

The systematic errors were estimated from the retrieval response to perturbations of the following parameters: pressure/temperature, O(^1D) and O(^3P) abundances, MIPAS gain calibration and solar flux. The magnitudes of these perturbations are the same as those used in the retrieval of the collisional rates in Jurado-Navarro et al. (2015), except for temperature that was assumed with an error of 5 K up to 100 km, 10 K between 100 and 110 km, and 15 K between 110 and 142 km, and for the LOS which was retrieved here. The other perturbations, which are discussed in detail in that reference are: 1.25% for the gain calibration; 1% for the solar flux; a 50% uncertainty in the concentration of O(^3P); and an uncertainty of 10% in the concentration of O(^1D) below 80 km and 30% above.

Atmos. Meas. Tech. Discuss., doi:10.5194/amt-2016-63, 2016
Manuscript under review for journal Atmos. Meas. Tech.
Published: 15 March 2016

Atmospheric Measurement Techniques Discussions

In addition, systematic CO_2 retrieval errors due to uncertainties in the collisional rates used in the non-LTE modeling need to be taken into account. However, since the CO_2 collisional parameters used here in the CO_2 inversion have been retrieved from MIPAS measurement in the same spectral region (see Jurado-Navarro et al., 2015), the CO_2 retrieval errors due to systematic errors of the retrieved rates are expected to be correlated with the errors caused by model parameter uncertainties. Therefore, adding the systematic errors due to collisional rate uncertainties quadratically to the other errors would not be adequate. For instance, it might occur that an overestimation of the solar flux introduces a low bias of a certain collisional rate, but the use of the underestimated rate in the CO_2 retrieval compensates the "direct" CO_2 error caused by assuming a too low solar flux. Therefore we calculate the $\Delta\mathrm{CO}_2(y_i)$ error due to a given model parameter, y_i, i.e., pressure/temperature, O(^1D), O(^3P), gain calibration and solar flux, by means of

$$\Delta\mathrm{CO}_2(y_i) = \left(\frac{\delta\mathrm{CO}_2}{\delta y_i}\right)_{\forall x_j = cte} \Delta y_i + \sum_j \left(\frac{\delta\mathrm{CO}_2}{\delta x_j}\right)\Delta x_j(y_i), \quad \text{with} \quad \Delta x_j(y_i) = \left(\frac{\delta x_j}{\delta y_i}\right)\Delta y_i, \tag{1}$$

where the second term in the righthand side accounts for the propagation of the error of model parameters, y_i, through the errors in the retrieved collisional parameters, $\Delta x_j(y_i)$. The sum extends over the retrieved collisional parameters, x_j: k_{vv2}, k_{vv3}, k_{vv4}, k_{F1}, k_{F2}, and f_{vt}, whose errors due to the model parameters y_i, $\Delta x_j(y_i)$, are listed in Table 3 of Jurado-Navarro et al. (2015). The first term in the righthand side, where Δy_i is the error of model parameter y_i, has been discussed above. The total systematic error in CO_2 is then calculated by a quadratic sum over the errors of all model parameters, $\Delta\mathrm{CO}_2^{\mathrm{Total}} = \sqrt{\sum_i [\Delta\mathrm{CO}_2(y_i)]^2}$.

The resulting corrected retrieval responses to the model parameter perturbations are shown in Figs. 8a and 8b and are listed in Table 1 for some altitudes.

The calculations indicate that the largest error contribution above 100 km comes from the pressure/temperature uncertainties for both considered atmospheric conditions, reaching values up to ∼12% in mid-latitude (Fig. 8a) and ∼16% in polar summer conditions (Fig. 8b). Below, the pressure/temperature error maximizes again around 80 km, with maximum values at mid-latitude conditions of up to ∼4%. The MIPAS gain calibration and solar flux uncertainties introduce errors of 2–3% from 85 up to 110 km in both conditions. The total error below 90 km in polar summer conditions is indeed dominated by these uncertainties. The O(^1D) and O(^3P) uncertainties have a non-negligible contribution above 95 km with largest values up to 4% at 105 km in polar summer conditions.

It is important to highlight that, in polar summer conditions, the MIPAS temperature retrieved from the NO 5.3 μm emission is smaller than MSIS temperatures in up to 10 K in the lower thermosphere (Bermejo-Pantaleón et al., 2011). Thus, the use of thermospheric MIPAS temperature, instead of MSIS, increases the retrieved CO_2 vmr by up to 15% under these particular conditions.

Regarding the effects of the joint CO_2-LOS retrieval on the total systematic error, Fig. 9 shows that it is notably larger for the CO_2-only retrieval than for the joint CO_2-LOS retrieval. This indicates that a large fraction of the spectral residuals due to the systematic errors of the different parameters is compensated by the LOS in the joint retrieval while in the CO_2-only retrieval all errors map onto the CO_2 vmr profile. In this sense, the joint CO_2-LOS retrieval is also useful to dampen systematic errors of the retrieved CO_2 vmr.

Atmos. Meas. Tech. Discuss., doi:10.5194/amt-2016-63, 2016
Manuscript under review for journal Atmos. Meas. Tech.
Published: 15 March 2016

Atmospheric Measurement Techniques Discussions

Deviations of the retrieved profile from the "true" profile when perturbing the *a priori* profile are often called smoothing errors. However, while it is important to assess the sensitivity of the retrieval to the *a priori* profile shape as we do above, we do not include smoothing errors in the overall error budget. First, because the concept of "smoothing errors" itself is questionable (von Clarmann, 2014), and secondly, because these deviations can be implicitly accounted for in comparisons to model simulations or independent observations by applying the MIPAS averaging kernels to the latter.

One important result that should be mentioned is that the systematic errors obtained here in the retrieved CO_2 vmr are much smaller than those obtained before in previous measurements of CO_2 using limb emission measurements of the 4.3 μm atmospheric radiance (e.g. López-Puertas et al., 1998; Kaufmann et al., 2002; Rezac et al., 2015). The main reasons are: first, the much more accurate non-LTE collisional rates that the high resolution MIPAS spectra have allowed us to retrieve previous to the CO_2 retrieval (see Jurado-Navarro et al., 2015); and, secondly, that the wide spectral range together with the high spectral resolution of MIPAS have allowed to retrieve, before the CO_2 vmr, the temperature and O_3 up to about 100 km, and the temperature in the lower thermosphere (up to ∼170 km). The use of these concentrations have reduced significantly the systematic error of CO_2.

6 MIPAS CO_2 climatology for 2010–2011

Figures 10a and 10b show the monthly zonal mean CO_2 vmr retrieved from MIPAS daytime spectra taken in its upper atmosphere (UA) mode. The figure shows the major features expected for the CO_2 distribution and predicted by models. Namely, the abrupt decline of the CO_2 vmr above around 80–90 km. The other major feature is the seasonal change of the latitudinal distribution, leading to higher CO_2 vmr from 70 up to ∼95 km in the polar summer, induced by the ascending branch of the mean circulation, and lower CO_2 abundances, with respect to the tropics and polar summer, at the same altitudes in the polar winter region. It is noticeable that the distribution reverses above ∼95 km, CO_2 being more abundant in the polar winter region than at mid-latitudes and polar summer; also as a consequence of the reversal of the mean circulation (see, e.g. Smith et al., 2011). The solstice seasonal distribution, with a significant pole-to-pole CO_2 gradient lasts about 2.5 months in each hemisphere (November through February, and May through August), while the seasonal transition occurs quickly, mainly in April and October.

Another observed feature is the rapid increase of CO_2 vmr from mid-high latitudes towards the polar regions in the lower thermosphere during equinoxes (more evident in April and October). We cannot find any physical reason for it and we do not discard that this could be a retrieval artifact caused by the inversion of CO_2 in conditions of very high ($>80°$) solar zenith angles.

A comparison of the MIPAS CO_2 vmr with ACE measurements for four days (two in solstice and two in equinox) have been presented in Jurado-Navarro et al. (2015), showing a good general agreement. A more detailed comparison with ACE data covering a more extended period as well as with SABER observations and with WACCM simulations is foreseen to be presented in future work.

Atmos. Meas. Tech. Discuss., doi:10.5194/amt-2016-63, 2016
Manuscript under review for journal Atmos. Meas. Tech.
Published: 15 March 2016

Atmospheric Measurement Techniques Discussions

7 Conclusions

We have retrieved global distributions of the CO_2 vmr (volume mixing ration) in the mesosphere and thermosphere (from 70 km up to ∼142 km) for MIPAS high resolution spectra. This is the first time that the relative CO_2 concentration (vmr) has been retrieved in the middle thermosphere (120–140 km). The retrieved CO_2 has an unprecedented accuracy because of the highly accurate rate coefficients recently derived from MIPAS (Jurado-Navarro et al., 2015), and the simultaneous MIPAS measurements of other key atmospheric parameters needed for the non-LTE modeling like the temperature in the mesosphere and in the thermosphere, as well as the O_3 concentration.

The CO_2 vmrs have been retrieved using MIPAS daytime limb emission spectra from the 4.3 μm region in its upper atmosphere (UA) mode (data version v5r_CO2_622). Nighttime spectra were not used because they are very noisy and the non-LTE processes operating at night are not known very accurately. The retrieved CO_2 covers from 70 km up to about 142 km and all latitudes except in the dark regions of the polar winter. The inversion of CO_2 has been performed jointly with the line of sight (LOS) by using a non-LTE retrieval scheme developed at IAA/IMK. It takes the advantage of other (simultaneous) MIPAS measurements of atmospheric parameters, as the kinetic temperature (up to ∼100 km) from the CO_2 15 μm region, the thermospheric temperature from the NO 5.3 μm, the O_3 measurements (up to ∼100 km), which allows a strong constrain of the O(^{1}D) concentration below ∼100 km, and an accurate calculation of O(^1D) above ∼100 km. The non-LTE model incorporates the accurate vibrational-vibrational and vibrational-translational collisional rates derived from the MIPAS spectra.

The precision of the retrieved CO_2 vmr profiles varies with altitude ranging from ∼1% below 90 km, to 5% around 120 km and larger than 10% above 130 km. The larger values at higher altitudes are due to the lower signal-to-noise ratio. There are very little latitudinal and seasonal variations of the precision, which are mainly driven by the solar illumination conditions. The retrieved CO_2 profiles have a vertical resolution of about 5–7 km below 120 km and between 10 and 20 km at 120–142 km.

Retrieval simulations performed with synthetic spectra have demonstrated that the developed CO_2-LOS joint retrieval allows to retrieve the CO_2 profile in the 70–140 km range with very high accuracy. The use of strongly perturbed *a priori* CO_2 and LOS information, results in very small different between the "true" and the retrieved profiles, generally smaller than 2–3% in mid-latitudes, and smaller than 2% (except near 95–110 km where it ranges at 2–4%) for polar summer conditions. The retrieval scheme clearly discriminates the information of CO_2 concentration from the LOS. The mapping of typical CO_2 *a priori* uncertainties on the LOS being very small (less than 20 m), and a deviation in the *a priori* LOS profile of 200 m introduces a change in the retrieved CO_2 profile smaller than 1–2%. We have also found that the systematic errors are significantly reduced when using the CO_2-LOS joint retrieval instead of the CO_2-only scheme.

The major systematic error source is the uncertainty of the pressure/temperature profiles, retrieved also from MIPAS spectra, near 15 μm below 100 km (García-Comas et al., 2014) and from 5.3 μm above 100 km Bermejo-Pantaleón et al. (2011). They can induce a systematic error of up to 15–16% above 100 km, and of ∼5% around 80 km at mid-latitude conditions. The systematic errors due to uncertainties of the O(^1D) and O(^3P) profiles are within 3–4% in the 100–120 km region. The errors due to uncertainties in the gain calibration and in the solar flux at 4.3 and 2.7 μm are within ∼2% at all altitudes.

The most important features observed on the retrieved CO_2 can be summarized as follows:

Atmos. Meas. Tech. Discuss., doi:10.5194/amt-2016-63, 2016
Manuscript under review for journal Atmos. Meas. Tech.
Published: 15 March 2016

– The retrieved CO_2 shows the major general features expected and predicted by models: the abrupt decline of the CO_2 vmr above 80–90 km, caused by the predominance of the molecular diffusion, and the seasonal change of the latitudinal distribution. The latter is reflected by higher CO_2 abundances in polar summer from 70 km up to ∼95 km, and lower CO_2 vmr in the polar winter, both induced by the ascending and descending branches of the mean circulation, respectively. Above ∼95 km, CO_2 is more abundant in the polar winter than at mid-latitudes and polar summer regions, caused by the reversal of the mean circulation in that altitude region.

– The solstice seasonal distribution, with a significant pole-to-pole CO_2 gradient lasts about 2.5 months in each hemisphere (November through February, and May through August), while the seasonal transition occurs quickly, mainly in April and October.

Acknowledgements. The IAA team was supported by the Spanish MCINN under grant ESP2014-54362-P and EC FEDER funds. M. García-Comas was financially supported by the Ministry of Economy and Competitiveness (MINECO) through its 'Ramón y Cajal' subprogram. The authors acknowledge ESA for providing MIPAS L1b spectra.

Atmos. Meas. Tech. Discuss., doi:10.5194/amt-2016-63, 2016
Manuscript under review for journal Atmos. Meas. Tech.
Published: 15 March 2016

Atmospheric Measurement Techniques Discussions

References

Beagley, S. R., Boone, C. D., Fomichev, V. I., Jin, J. J., Semeniuk, K., McConnell, J. C., and Bernath, P. F.: First multi-year occultation observations of CO_2 in the MLT by ACE satellite: observations and analysis using the extended CMAM, Atmospheric Chemistry and Physics, 10, 1133–1153, doi:10.5194/acp-10-1133-2010, 2010.

Bermejo-Pantaleón, D., Funke, B., Lopez-Puertas, M., García-Comas, M., Stiller, G. P., von Clarmann, T., Linden, A., Grabowski, U., Höpfner, M., Kiefer, M., Glatthor, N., Kellmann, S., and Lu, G.: Global Observations of Thermospheric Temperature and Nitric Oxide from MIPAS spectra at 5.3 μm, J. Geophys. Res., 116, A10 313, 2011.

De Laurentis, M.: Planning of MIPAS new special modes January 2005 Campaign, Tech. rep., ESA Technical Note, ENVI-SPPA-EOPG-TN-05-0002, 2005.

Fischer, H., Birk, M., Blom, C., Carli, B., Carlotti, M., von Clarmann, T., Delbouille, L., Dudhia, A., Ehhalt, D., Endemann, M., Flaud, J. M., Gessner, R., Kleinert, A., Koopman, R., Langen, J., López-Puertas, M., Mosner, P., Nett, H., Oelhaf, H., Perron, G., Remedios, J., Ridolfi, M., Stiller, G., and Zander, R.: MIPAS: an instrument for atmospheric and climate research, Atmospheric Chemistry and Physics, 8, 2151–2188, doi:10.5194/acp-8-2151-2008, http://www.atmos-chem-phys.net/8/2151/2008/, 2008.

Funke, B., López-Puertas, M., Stiller, G. P., von Clarmann, T., and Höpfner, M.: A new non–LTE Retrieval Method for Atmospheric Parameters From MIPAS–ENVISAT Emission Spectra, Adv. Space Res., 27, 1099–1104, doi:10.1016/S0273-1177(01)00169-7, 2001.

Funke, B., López-Puertas, M., García-Comas, M., Kaufmann, M., Höpfner, M., and Stiller, G. P.: GRANADA: A Generic RAdiative traNsfer AnD non-LTE population algorithm, JQRST, 113, 1771–1817, doi:10.1016/j.jqsrt.2012.05.001, 2012.

Funke, B., López-Puertas, M., García-Comas, M., Kaufmann, M., Höpfner, M., and Stiller, G. P.: GRANADA: a Generic RAdiative traNsfer AnD non-LTE population Algorithm, J. Quant. Spectrosc. Radiat. Transfer, 113, 1771–1817, doi:10.1016/j.jqsrt.2012.05.001, http://dx.doi.org/10.1016/j.jqsrt.2012.05.001, 2012.

Garcia, R. R., López-Puertas, M., Funke, B., Marsh, D. R., Kinnison, D. E., Smith, A. K., and González-Galindo, F.: On the distribution of CO_2 and CO in the mesosphere and lower thermosphere, Journal of Geophysical Research: Atmospheres, 119, 5700–5718, doi:10.1002/2013JD021208, 2014.

García-Comas, M., Funke, B., Gardini, A., López-Puertas, M., Jurado-Navarro, A., von Clarmann, T., Stiller, G., Kiefer, M., Boone, C. D., Leblanc, T., Marshall, B. T., Schwartz, M. J., and Sheese, P. E.: MIPAS temperature from the stratosphere to the lower thermosphere: Comparison of vM21 with ACE-FTS, MLS, OSIRIS, SABER, SOFIE and lidar measurements, Atmospheric Measurement Techniques, 7, 3633–3651, doi:10.5194/amt-7-3633-2014, 2014.

Gil-López, S., López-Puertas, M., Kaufmann, M., Funke, B., García-Comas, M., Koukouli, M. E., Glatthor, N., Grabowski, U., Höpfner, Stiller, G. P., and von Clarmann, T.: Retrieval of stratospheric and mesospheric O_3 from high resolution MIPAS spectra at 15 and 10 μm, Adv. Space Res., 36, 943–951, doi:10.1016/j.asr.2005.05.123, 2005.

González-Galindo, F., López-Valverde, M. A., Angelats i Coll, M., and Forget, F.: Extension of a Martian general circulation model to thermospheric altitudes: UV heating and photochemical models, Journal of Geophysical Research, 110, 09 008, 2005.

Jurado-Navarro, Á. A., López-Puertas, M., Funke, B., García-Comas, M., Gardini, A., Stiller, G. P., and Clarmann, T. v.: Vibrational-vibrational and vibrational-thermal energy transfers of CO2 with N2 from MIPAS high-resolution limb spectra, Journal of Geophysical Research: Atmospheres, 120, 8002–8022, doi:10.1002/2015JD023429, http://dx.doi.org/10.1002/2015JD023429, 2015JD023429, 2015.

Kaufmann, M., Gusev, O. A., Grossmann, K. U., Roble, R. G., Hagan, M. E., Hartsough, C., and Kutepov, A. A.: The vertical and horizontal distribution of CO_2 densities in the upper mesosphere and lower thermosphere as measured by CRISTA, Journal of Geophysical Research: Atmospheres, 107, CRI 10–1–CRI 10–19, doi:10.1029/2001JD000704, 2002.

Lean, J., Rottman, G., Harder, J., and Kopp, G.: SORCE Contributions to New Understanding of Global Change and Solar Variability, Solar Physics, 230, 27–53, 2005.

López-Puertas, M. and Taylor, F. W.: Non-LTE radiative transfer in the Atmosphere, World Scientific Pub., Singapore, 2001.

López-Puertas, M., Zaragoza, G., López-Valverde, M. Á., and Taylor, F. W.: Non local thermodynamic equilibrium (LTE) atmospheric limb emission at 4.6 μm 2. An analysis of the daytime wideband radiances as measured by UARS improved stratospheric and mesospheric sounder, J. Geophys. Res., 103, 8515–8530, 1998.

López-Puertas, M., López-Valverde, M. Á., Garcia, R. R., and Roble, R. G.: A review of CO_2 and CO abundances in the middle atmosphere, in: Atmospheric Science Across the Stratopause, edited by Siskind, D. E., Eckermann, S. D., and Summers, M. E., vol. 123 of *Geophysical Monograph Series*, p. 83, American Geophysical Union, 2000.

Lu, H. C., Chen, H. K., Chen, H. F., Cheng, B. M., and Ogilvie, J. F.: Absorption cross section of molecular oxygen in the transition $E^3\Sigma_u^- v$= 0–$X^3\Sigma_g^-$ v= 0 at 38 K, Astronomy and Astrophysics, 520, A19, 2010.

Oelhaf, H.: MIPAS Mission Plan, ESA Technical Note ENVI-SPPA-EOPG-TN-07-0073, 2008.

Offermann, D. and Grossmann, K. U.: Thermospheric density and composition as determined by a mass spectrometer with cryo ion source, Journal of Geophysical Research, 78, 8296–8304, doi:10.1029/JA078i034p08296, 1973.

Ogawa, S. and Ogawa, M.: Absorption Cross Sections of $O_2(a^1\Delta_g)$ and $O_2(X^3\Sigma_g^-)$ in the Region from 1087 to 1700 Å, Canadian Journal of Physics, 53, 1845–1852, 1975.

Perron, G., Aubertin, G., Desbiens, R., Fehr, T., Niro, F., Kleinert, A., Kiefer, M., Birk, M., and Wagner, G.: MIPAS Level 1b Algorithm Evolutions, in: ESA Living Planet Symposium 2010 (Bergen, Norway), vol. SP-686, ESA Publication Division, 2010.

Picone, J., Hedin, A., Drob, D., and Aikin, A.: NRLMSISE-00 empirical model of the atmosphere: Statistical comparisons and scientific issues, J. Geophys. Res., 107, 1468, doi:10.1029/2002JA009 430, 2002.

Raspollini, P., Carli, B., Ceccherini, S., Forzieri, G., Sgheri, L., Ridolfi, M., Carlotti, M., Papandrea, E., Arnone, E., Dinelli, B. M., Castelli, E., Remedios, J., Sembhi, H., Dudhia, A., Lopez-Puertas, M., Funke, B., Flaud, J.-M., von Clarmann, T., Hoepfner, M., Oelhaf, H., Fischer, H., Kiefer, M., Kleinert, A., Chipperfield, M., .Perron, G., Aubertin, G., Birk, M., Wagner, G., Gessner, R., Mosner, P., Schmitt, M., Fehr, T., D'Alba, L., and Niro, F.: Level 2 near–real–time analysis of MIPAS measurements on ENVISAT, in: Eight years of MIPAS measurements, vol. SP-686, pp. 011–d2, ESA Publication Division, 2010.

Rezac, L., Kutepov, A., III, J. R., Feofilov, A., Yue, J., and Goldberg, R.: Simultaneous retrieval of T(p) and CO_2 VMR from two-channel non-LTE limb radiances and application to daytime SABER/TIMED measurements, Journal of Atmospheric and Solar-Terrestrial Physics, 130-131, 23–42, doi:http://dx.doi.org/10.1016/j.jastp.2015.05.004, 2015.

Rienecker, M. M., Suarez, M. J., Gelaro, R., Todling, R., Bacmeister, J., Liu, E., Bosilovich, M. G., Schubert, S. D., Takacs, L., Kim, G.-K., Bloom, S., Chen, J., Collins, D., Conaty, A., da Silva, A., Gu, W., Joiner, J., Koster, R. D., Lucchesi, R., Molod, A., Owens, T., Pawson, S., Pegion, P., Redder, C. R., Reichle, R., Robertson, F. R., Ruddick, A. G., Sienkiewicz, M., and Woollen, J.: MERRA: NASA's Modern-Era Retrospective Analysis for Research and Applications, J. Climate, 24, 3624–3648, doi:10.1175/jcli-d-11-00015.1, http://dx.doi.org/10.1175/jcli-d-11-00015.1, 2011.

Smith, A. K., Garcia, R. R., Marsh, D. R., and Richter, J. H.: WACCM simulations of the mean circulation and trace species transport in the winter mesosphere, Journal of Geophysical Research, 116, D20 115, 2011.

Stair, A. T., Sharma, R. D., Nadile, R. M., Baker, D. J., and Grieder, W. F.: Observations of limb radiance with Cryogenic Spectral Infrared Rocket Experiment, Journal of Geophysical Research: Space Physics, 90, 9763–9775, doi:10.1029/JA090iA10p09763, 1985.

Stiller, G. P., von Clarmann, T., Funke, B., Glatthor, N., Hase, F., Höpfner, M., and Linden, A.: Sensitivity of trace gas abundances retrievals from infrared limb emission spectra to simplifying approximations in radiative transfer modelling, J. Quant. Spectrosc. Radiat. Transfer, 72, 249–280, doi:10.1016/S0022-4073(01)00123-6, 2002.

Tikhonov, A.: On the solution of incorrectly stated problems and method of regularization, Dokl. Akad. Nauk. USSR, 151, 501–504, 1963.

Trinks, H. and Fricke, K. H.: Carbon dioxide concentrations in the lower thermosphere, Journal of Geophysical Research: Space Physics, 83, 3883–3886, doi:10.1029/JA083iA08p03883, 1978.

Trinks, H., Offermann, D., von Zahn, U., and Steinhauer, C.: Neutral composition measurements between 90 and 220 km altitude by rocket-borne mass spectrometer, Journal of Geophysical Research: Space Physics, 83, 2169–2176, doi:10.1029/JA083iA05p02169, 1978.

von Clarmann, T.: Smoothing error pitfalls, Atmospheric Measurement Techniques, 7, 3023–3034, doi:10.5194/amt-7-3023-2014, 2014.

von Clarmann, T. and Echle, G.: Selection of optimized microwindows for atmospheric spectroscopy, Appl. Opt., 37, 7661–7669, 1998.

von Clarmann, T., Glatthor, N., Grabowski, U., Höpfner, M., Kellmann, S., Kiefer, M., Linden, A., Mengistu Tsidu, G., Milz, M., Steck, T., Stiller, G. P., Wang, D. Y., Fischer, H., Funke, B., Gil-López, S., and López-Puertas, M.: Retrieval of temperature and tangent altitude pointing from limb emission spectra recorded from space by the Michelson Interferometer for Passive Atmospheric Sounding (MIPAS), J. Geophys. Res., 108, 4736, doi:10.1029/2003JD003602, 2003.

Whitson, M. E. and McNeal, R. J.: Temperature dependence of the quenching of vibrationally excited N_2 by NO and H_2O, The Journal of Chemical Physics, 66, 2696–2700, doi:http://dx.doi.org/10.1063/1.434217, 1977.

Zaragoza, G., López-Puertas, M., López-Valverde, M., and Taylor, F. W.: Global distribution of CO_2 in the upper mesosphere as derived from UARS/ISAMS measurements, Journal of Geophysical Research: Atmospheres, 105, 19 829–19 839, doi:10.1029/2000JD900243, 2000.

Atmos. Meas. Tech. Discuss., doi:10.5194/amt-2016-63, 2016
Manuscript under review for journal Atmos. Meas. Tech.
Published: 15 March 2016

Atmospheric Measurement Techniques Discussions

Table 1. Errors of the CO_2 vmr retrieved in this work for mid-latitudes and for polar summer (in parenthesis) conditions.

Height (km)	Errors (%)						
	Random	Pressure/Temp.	O(^1D)	O(^3P)	Gain (1.25%)	Solar flux (1%)	Total
70	<1 (<1)	0.33 (0.05)	0.14 (0.17)	0.10 (0.09)	0.08 (0.18)	0.03 (0.12)	0.38 (0.3)
75	1 (1)	3.3 (0.36)	1.2 (1.6)	0.8 (0.7)	0.7 (1.7)	0.24 (1.2)	3.7 (2.7)
80	1 (1)	5.1 (0.38)	1.4 (1.8)	0.44 (0.4)	0.8 (2.0)	0.02 (1.1)	5.4 (3.0)
85	1 (1)	3.2 (0.9)	1.2 (1.3)	0.12 (0.17)	0.67 (1.1)	0.19 (0.18)	3.5 (2.0)
90	2 (2)	1.5 (0.6)	1.4 (1.4)	0.44 (0.16)	0.8 (1.1)	0.16 (0.12)	2.3 (1.8)
95	3 (3)	1.0 (6)	1.0 (0.6)	0.03 (0.9)	0.45 (0.08)	0.6 (1.2)	1.6 (6)
100	3 (3)	4.4 (13)	1.1 (4)	1.4 (3.4)	0.34 (2.0)	1.4 (2.8)	5 (15)
105	4 (4)	9 (14)	2.5 (4)	1.6 (3.5)	0.6 (1.8)	1.4 (2.2)	10 (16)
110	5 (4)	11 (13)	3.1 (3.2)	2.5 (3.4)	0.9 (1.3)	1.4 (1.7)	12 (14)
115	5 (5)	10 (13)	1.1 (1.6)	2.2 (2.7)	0.01 (0.34)	0.7 (0.9)	11 (13)
120	6 (5)	11 (14)	0.6 (0.6)	0.8 (2.0)	0.8 (0.02)	0.02 (0.6)	11 (14)
125	7 (7)	12 (15)	1.2 (0.3)	0.13 (1.0)	0.9 (0.31)	0.25 (0.32)	12 (15)
130	9 (9)	13 (16)	1.5 (1.1)	0.9 (0.06)	1.1 (0.6)	0.4 (0.07)	13 (16)
135	11 (12)	13 (16)	2.1 (1.7)	2.1 (0.9)	1.5 (0.9)	0.7 (0.13)	14 (16)
140	13 (14)	14 (16)	2.8 (2.2)	3.4 (1.5)	1.2 (1.1)	1.1 (0.28)	14 (16)

Atmos. Meas. Tech. Discuss., doi:10.5194/amt-2016-63, 2016
Manuscript under review for journal Atmos. Meas. Tech.
Published: 15 March 2016

Atmospheric Measurement Techniques Discussions

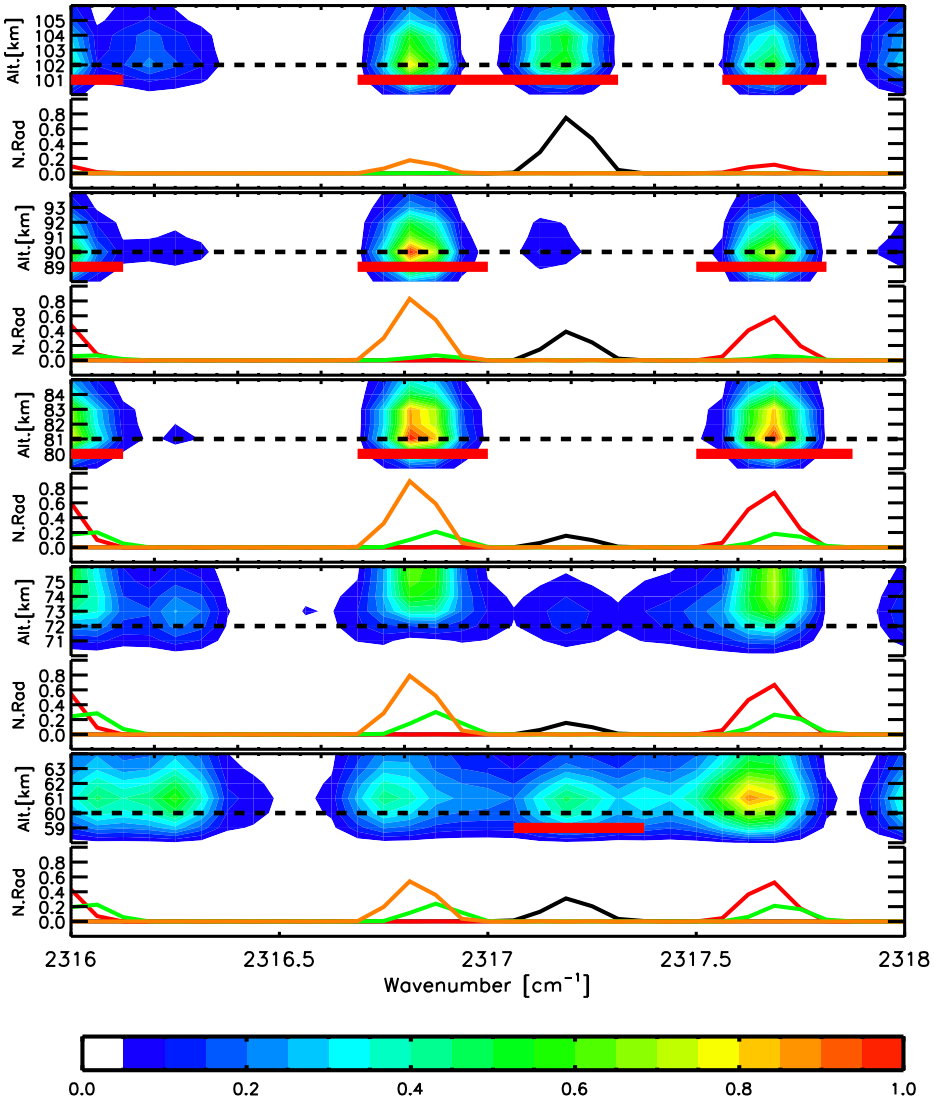

Figure 1. Jacobians and radiance for several lines in the 2316-2318 cm^{-1} region for five different tangent altitudes (from bottom to top: 60, 72, 81, 90 and 102 km). Two panels are shown for each tangent altitude. Upper panel: normalized Jacobians at the corresponding tangent height; dashed black line stands for the tangent altitude and thick red line for the microwindow mask. Lower panel: normalized radiance contributions for different lines of CO_2 bands; a line of the fundamental band in black, of the second hot $10^01 \rightarrow 10^00$ band in red, of the $02^21 \rightarrow 02^20$ band in green, and of $02^01 \rightarrow 02^00$ in orange.

Atmos. Meas. Tech. Discuss., doi:10.5194/amt-2016-63, 2016
Manuscript under review for journal Atmos. Meas. Tech.
Published: 15 March 2016

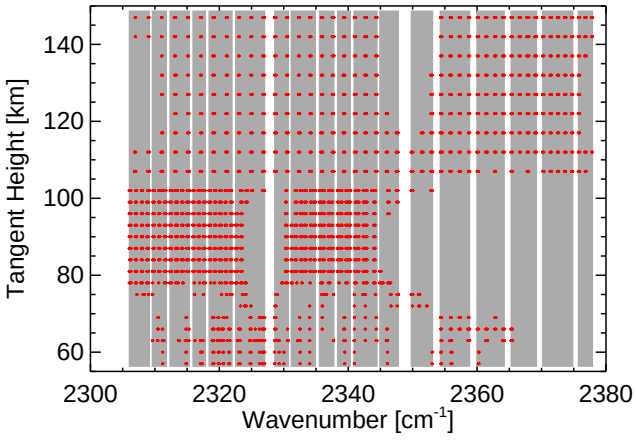

Figure 2. Occupation matrix used in the CO_2 retrieval in the 4.3 μm spectral region. Shaded regions represent the spectral regions selected and red dots the microwindow mask at each tangent height. The specific microwindows used in the retrieval are listed in the Supplement.

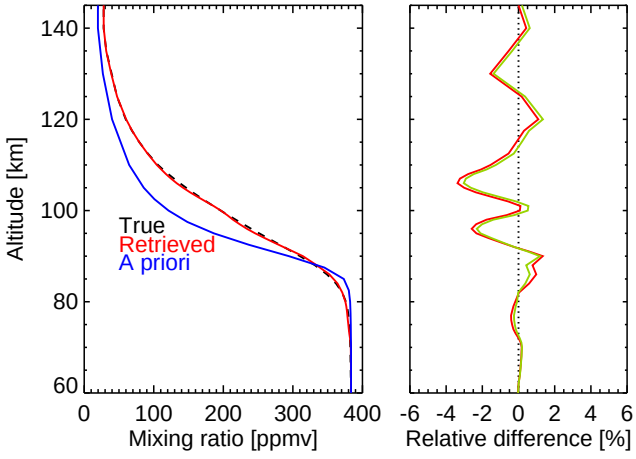

Figure 3a. Sensitivity of the retrieved CO_2 profile to the *a priori* CO_2 profile for mid-latitudes conditions. The relative differences (right panel) are referred to the CO_2/LOS joint retrieval (red solid line) and to the single-parameter CO_2 retrieval (green line).

Atmos. Meas. Tech. Discuss., doi:10.5194/amt-2016-63, 2016
Manuscript under review for journal Atmos. Meas. Tech.
Published: 15 March 2016

Atmospheric Measurement Techniques Discussions

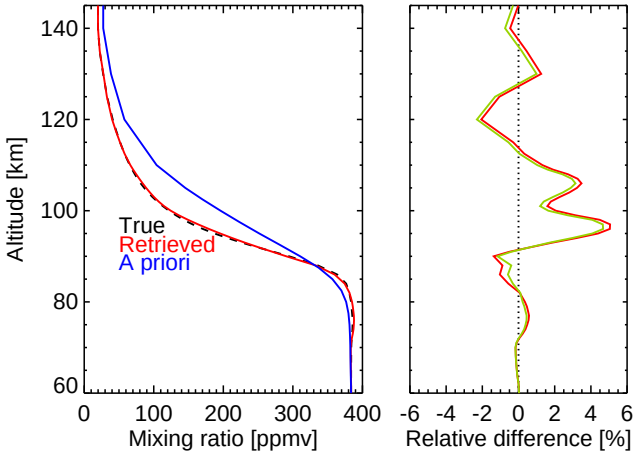

Figure 3b. As Fig. 3a but for polar summer conditions.

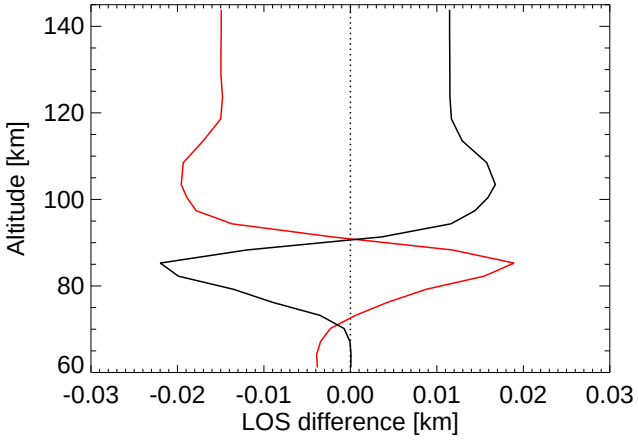

Figure 4. Sensitivity of the retrieved LOS (from the CO_2–LOS joint retrieval) to the CO_2 *a priori* uncertainties for mid-latitude (red) and polar summer (black) conditions. The lines show the retrieved–true LOS differences.

Atmos. Meas. Tech. Discuss., doi:10.5194/amt-2016-63, 2016
Manuscript under review for journal Atmos. Meas. Tech.
Published: 15 March 2016

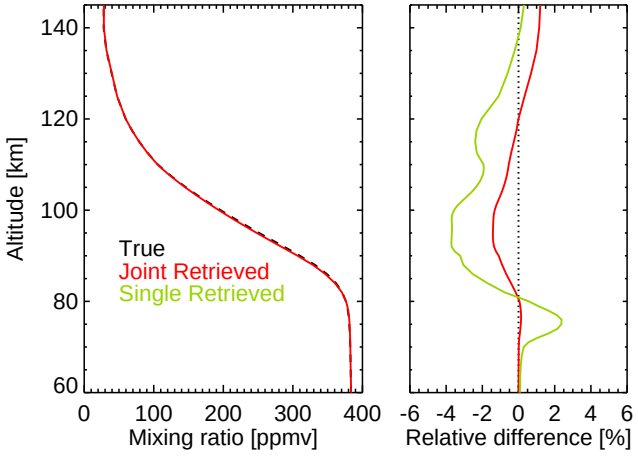

Figure 5a. Sensitivity of the retrieved CO_2 to LOS *a priori* uncertainties for mid-latitude conditions. The relative differences (retrieved–true) (right panel) are referred to the joint CO_2-LOS retrieval (red solid line) and to the single-parameter CO_2 retrieval (green line).

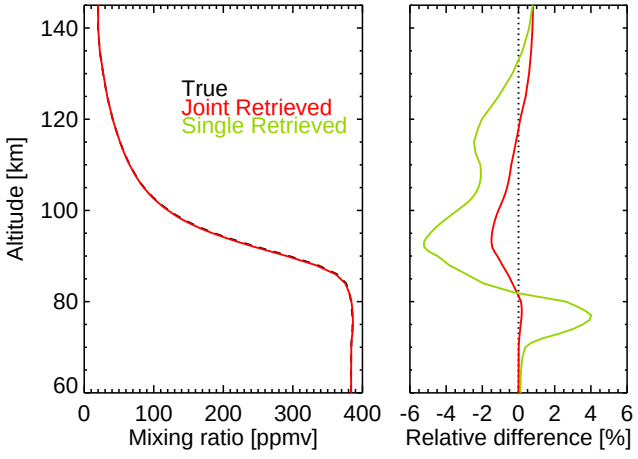

Figure 5b. As Fig. 5a but for polar summer conditions.

Atmos. Meas. Tech. Discuss., doi:10.5194/amt-2016-63, 2016
Manuscript under review for journal Atmos. Meas. Tech.
Published: 15 March 2016

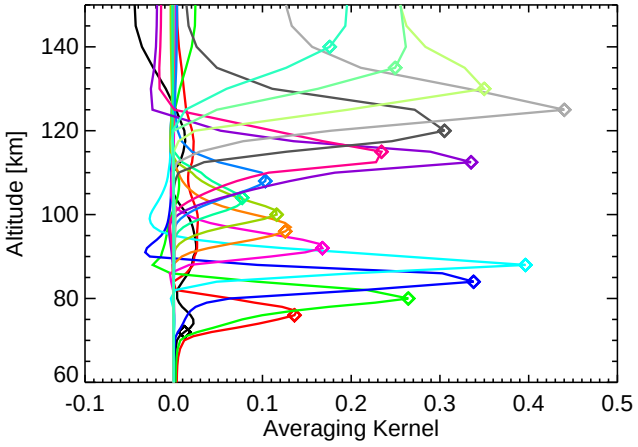

Figure 6a. Columns of the averaging kernel of the CO_2 vmr from the joint CO_2-LOS retrieval for mid-latitudes conditions.

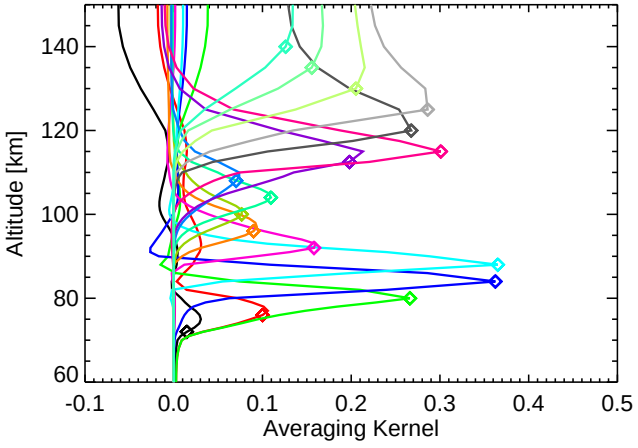

Figure 6b. As Fig. 6a but for polar summer conditions.

Atmos. Meas. Tech. Discuss., doi:10.5194/amt-2016-63, 2016
Manuscript under review for journal Atmos. Meas. Tech.
Published: 15 March 2016

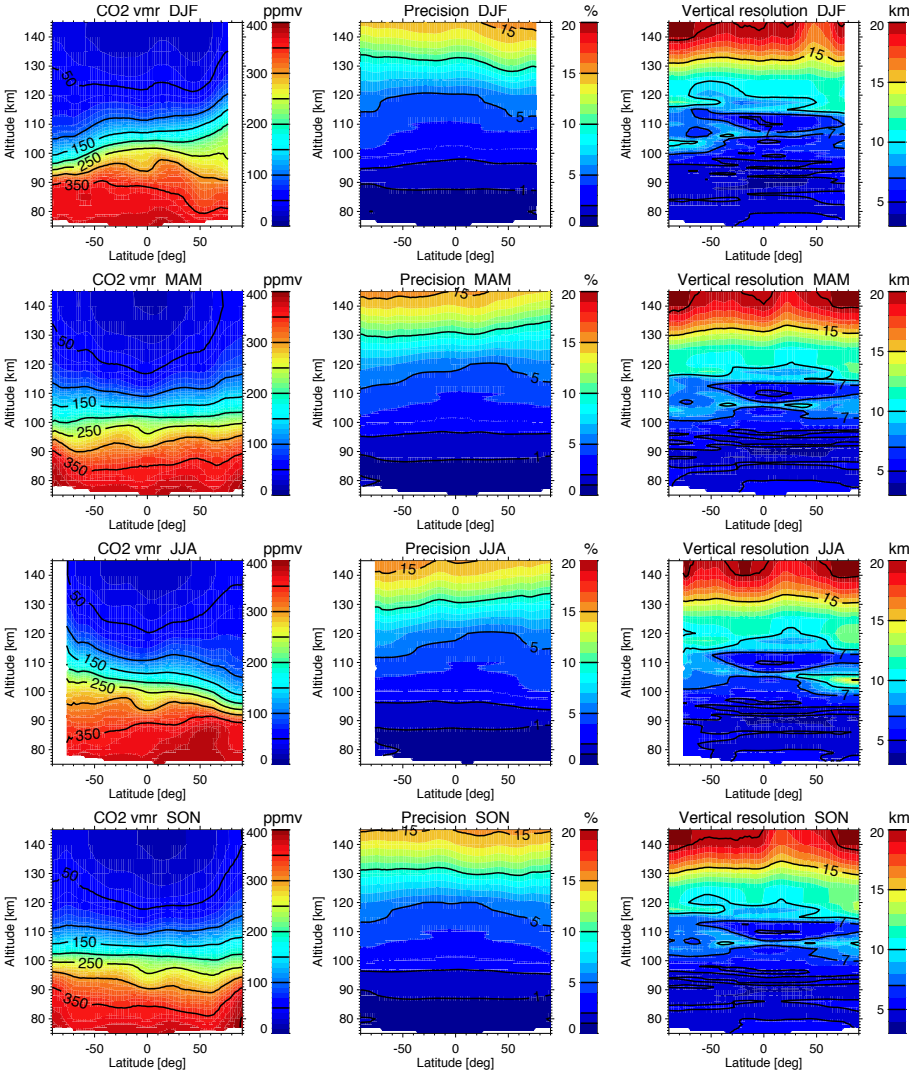

Figure 7. Latitude-altitude cross sections of CO_2 vmr (left column), precision (centre column) and vertical resolution (right column). The rows, from top to bottom, correspond to the boreal winter (DJF: December-January-February), the vernal equinox (MAM: March-April-May), the austral winter (JJA: June-July-August) and the autumnal equinox (SON: September-October-November). The MIPAS data include the measurements taken in 2010 and 2011 in the UA mode.

Atmos. Meas. Tech. Discuss., doi:10.5194/amt-2016-63, 2016
Manuscript under review for journal Atmos. Meas. Tech.
Published: 15 March 2016

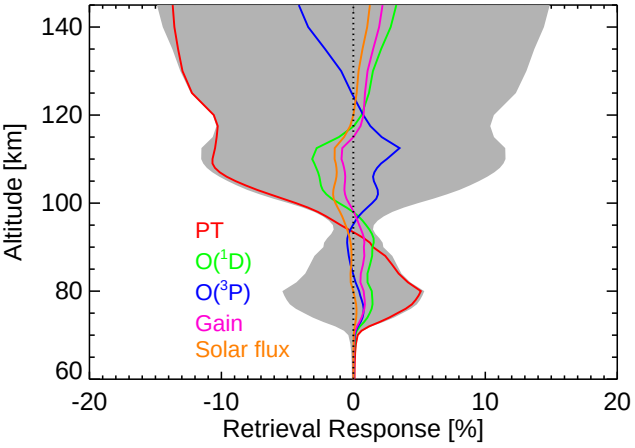

Figure 8a. Systematic errors of the CO_2 vmr introduced by different error sources for mid-latitude conditions. CO_2 retrieval responses to individual model parameter perturbations (reflecting their estimated uncertainties) are shown by the colored lines. The shaded area represents the total systematic error.

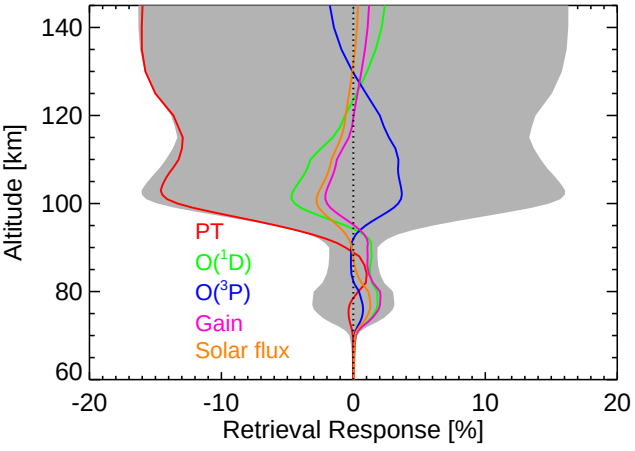

Figure 8b. As Fig. 8a but for polar summer conditions.

Atmos. Meas. Tech. Discuss., doi:10.5194/amt-2016-63, 2016
Manuscript under review for journal Atmos. Meas. Tech.
Published: 15 March 2016

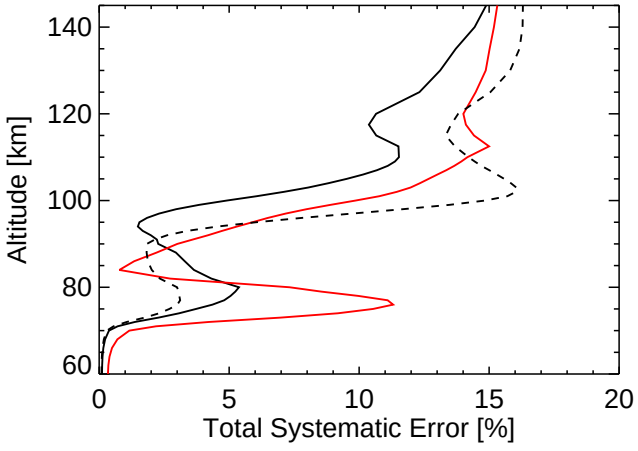

Figure 9. Total systematic errors of the main atmospheric parameters from the joint CO_2-LOS (black solid line) and CO_2-only (red line) retrievals for mid-latitude conditions. The dash black line shows the total systematic error of the joint CO_2-LOS retrieval for polar summer. The total errors are calculated from the quadratic sum of the retrieval responses to individual model parameter perturbations shown in Figs. 8a and 8b.

Atmos. Meas. Tech. Discuss., doi:10.5194/amt-2016-63, 2016
Manuscript under review for journal Atmos. Meas. Tech.
Published: 15 March 2016

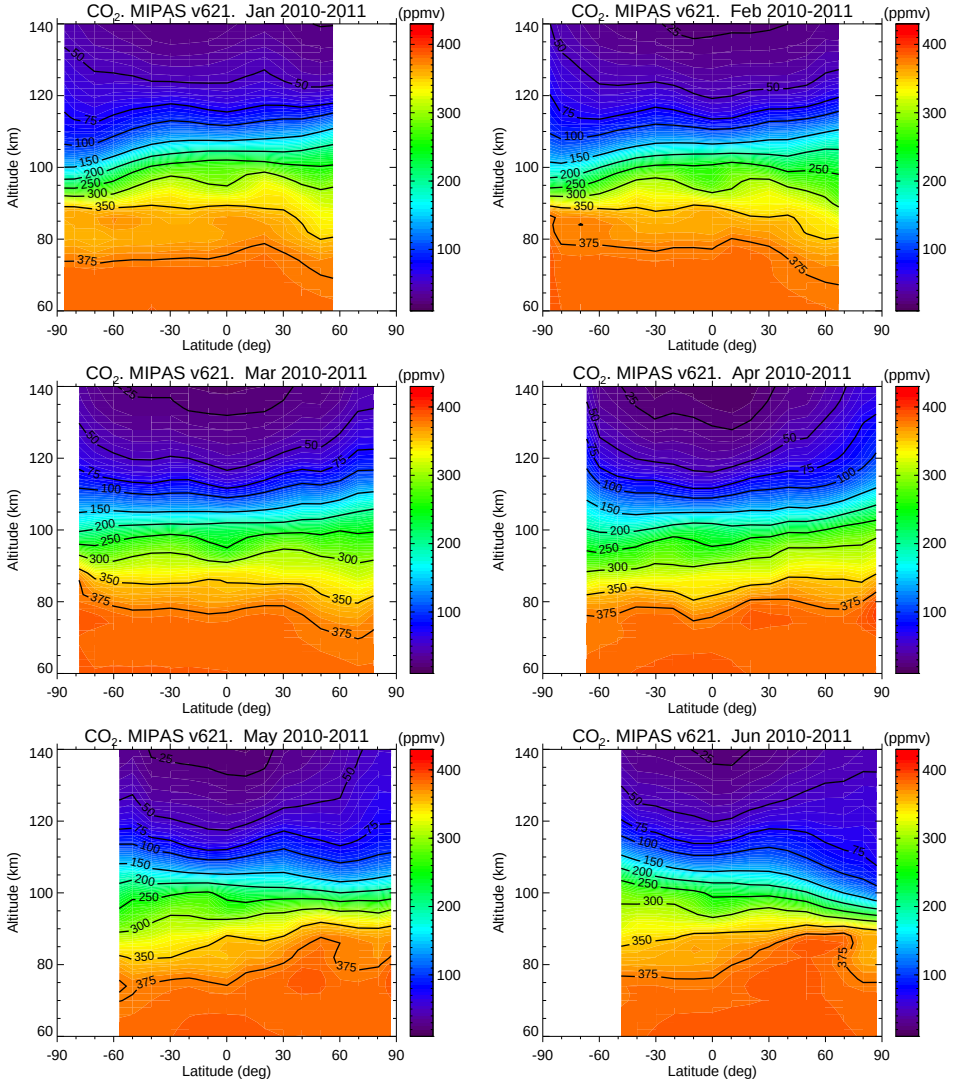

Figure 10a. Monthly zonal mean CO_2 vmr measured by MIPAS during the 2010–2011 period for the UA mode for months of January through June.

Atmos. Meas. Tech. Discuss., doi:10.5194/amt-2016-63, 2016
Manuscript under review for journal Atmos. Meas. Tech.
Published: 15 March 2016

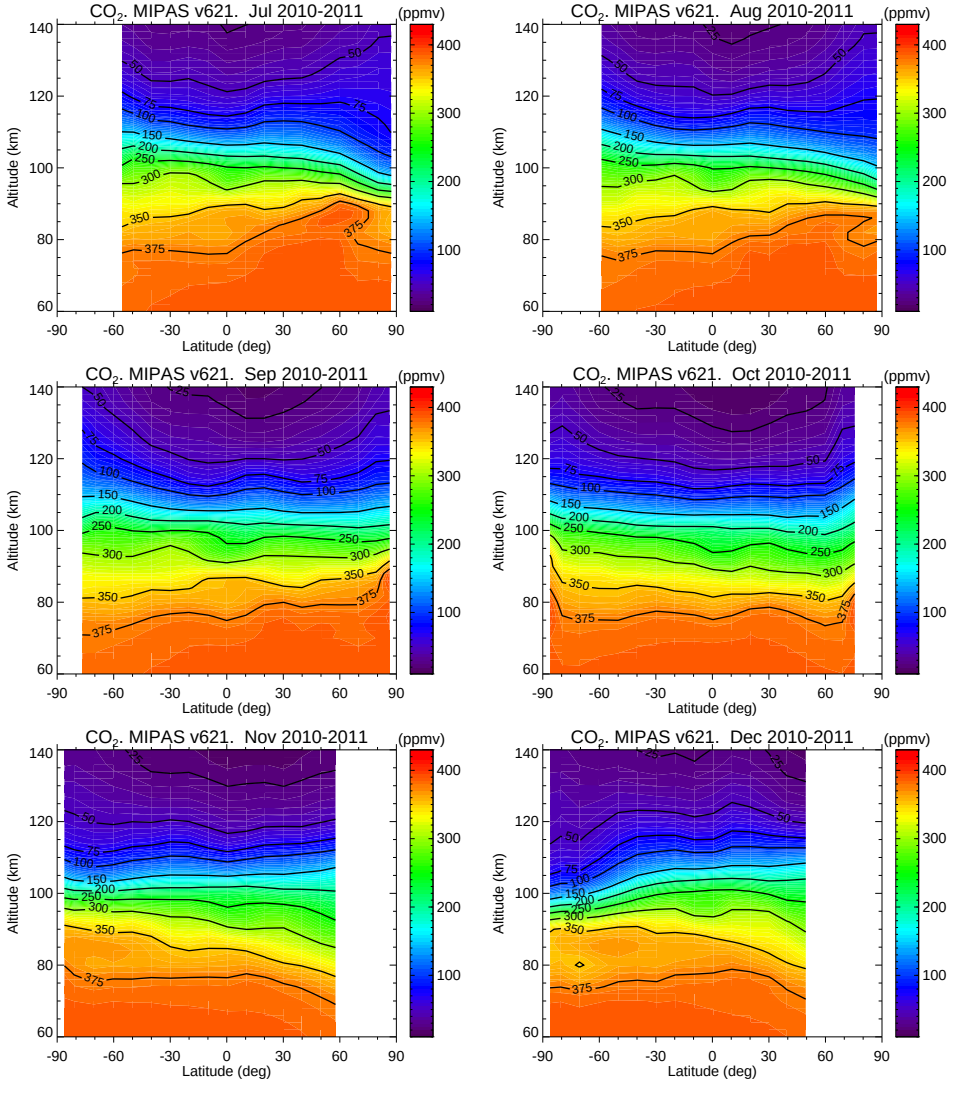

Figure 10b. As Fig. 10a but for months of July through December.